Absorption spectroscopy and time-dependent theoretical calculation of the intervalence band of $[Fe^{II}Fe^{III}BPMP(OPr)_2](BPh_4)_2$, a localized mixed-valence compound with a nonlinear metal-bridging ligand-metal core

Myriam Triest, Martin J. Davis and Christian Reber*

Département de Chimie, Université de Montréal, Montréal, QC H3C 3J7, Canada.
E-mail: reber@chimie.umontreal.ca

Received* (*in New Haven*) *7th December 1998, Accepted 8th February 1999

The title compound shows an intervalence absorption band in the near-infrared spectral region with a maximum at 8400 cm^{-1} at 80 K, as measured on a crystalline sample. The band has a width of 4750 cm^{-1} and is asymmetric. The molecule does not have a linear metal-bridging ligand-metal structure, a distinct difference to the vast majority of mixed-valence compounds studied by absorption spectroscopy. A one-dimensional model using coupled potential energy surfaces and a non-constant transition dipole moment varying along the configurational coordinate Q is presented, consistent with the symmetry of the title compound. We calculate the absorption band shape and its temperature dependence using a time-dependent theoretical approach. Our calculations show that the variation of the dipole moment along Q cannot be neglected in the analysis of the full absorption spectrum.

Mixed-valence compounds contain sites with formally different oxidation states. The best known representatives are bimetallic complexes, such as the Creutz–Taube compound,[1] $[(NH_3)_5Ru(C_4H_4N_2)Ru(NH_3)_5]^{5+}$. The electron transfer between the two metal ions in mixed-valence complexes is one of the simplest charge transfers possible. This is the main reason for the vast literature[2–6] aimed at the study of parameters that define the electron transfer processes in mixed-valence compounds. A better understanding of electron transfer has been obtained over the past years from both theoretical and experimental studies. Mixed-valence compounds are used as simple models of the reactivity of metal sites in proteins,[7–9] they also show interesting nonlinear optical properties,[10] they are candidates for molecular switches,[11] and the superconducting behavior of some compounds has been investigated.[12]

One of the first models for the intervalence transition was described by Hush[6] as a set of two one-dimensional potential curves with their minima displaced along the (horizontal) coordinate axis. An electron transfer from one site to the other is represented as a vertical electronic transition between the potential curves, an intriguing situation because the potentials can be coupled. Robin and Day[13] classified mixed-valence compounds in three categories: class I, completely valence trapped (no coupling between the potential curves); class II valence trapped (weak coupling between the potential curves); and class III, delocalized valency (strong coupling between the potential curves), implying that the two metal ions are indistinguishable. The Hush model provides us with relations between several model parameters like the reorganization energy or the coupling between the potential surfaces and experimental quantities of the intervalence band such as the wavenumber of its maximum, its width and its molar absorptivity. The model has been refined and extended to include solvent effects[4] and different types of bridging ligands.[14,15] The Hush model is widely used to describe localized compounds with a linear metal-bridging ligand-metal structure, such as the 4,4′-bipyridine-bridged analog of the Creutz–Taube ion.[2,3,5,16] Aspects such as the influence of the bridging ligands on the localized or delocalized nature of compounds (class II and III in the classification scheme of Robin and Day) can be determined,[17,18] but the model is not always successful in reproducing full intervalence band shapes.

More advanced models, such as the approach proposed by Schatz and coworkers,[19,20] include vibronic coupling to one or several vibrational modes, and the nature of the bridging ligands is explicitly considered in some calculations.[21–23] These models reproduce the absorption spectrum of the Creutz–Taube compound and similar molecules with a center of inversion relating the two metal ions, but appear to fail to reproduce the absorption spectrum of more complicated systems, such as a photosynthetic bacterial reaction center,[24,25] and tend to lead to parameters that are only in qualitative agreement with experimental quantities.[26] In a recent paper[27] anharmonic potential curves replaced the initially proposed harmonic surfaces.

The aim of this work is to investigate the intervalence absorption spectrum of a localized mixed-valence compound with a nonlinear bridging structure, a situation not investigated in detail in the existing literature. We use an approach recently developed by Talaga and Zink[28] to calculate intervalence spectra using time-dependent theoretical methods, based on a numerical solution of the time-dependent Schrödinger equation for coupled potential surfaces. Our model uses a coordinate-dependent transition dipole moment and harmonic potential surfaces displaced along the configurational coordinate. In order to reproduce the experimental spectrum it is essential explicitly to include the transition dipole moment. The restrictions imposed by symmetry and the resulting spectroscopic effects have been discussed in detail by Talaga and Zink.[28] This simplified, one-dimensional model is adequate for determining a number of characteristics of intervalence absorption spectra.

The complex used in the following is bis(μ-propionato-*O*,*O*′)(2,6-bis[{bis(2-pyridylmethyl)amino}methyl]-4-ethylphenolato)-diiron(II,III) bis(tetraphenylborate), abbreviated as $[Fe^{II}Fe^{III}BPMP(OPr)_2](BPh_4)_2$, a class II mixed-valence compound. We chose this compound for our study since the chemical nature of the ligands is identical for both iron ions, but X-ray crystallography shows different structural environ-

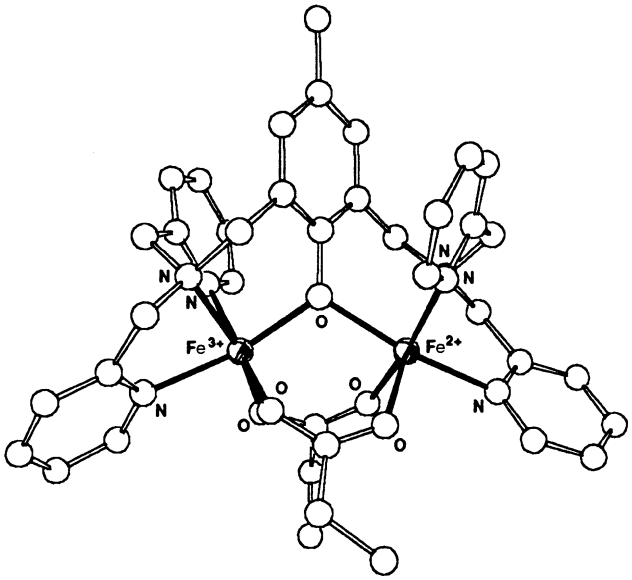

Fig. 1 The bimetallic molecular unit of $[Fe^{II}Fe^{III}BPMP(OPr_2)]^{2+}$. The atomic coordinates were taken from ref. 7.

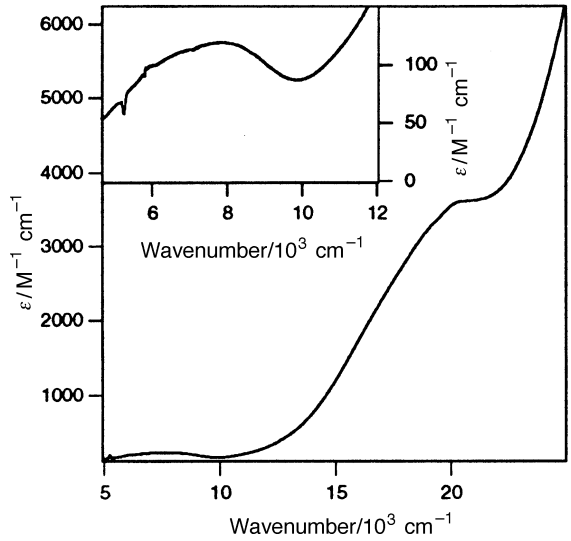

Fig. 2 The absorption spectrum of $[Fe^{II}Fe^{III}BPMP(OPr_2)]^{2+}$ in acetone solution. The inset shows the intervalence band in d_3-acetonitrile.

ments for the two centers. It is therefore a molecule with interchange symmetry, which is not the case for the large number of class II mixed-valence compounds with different ligand spheres for the two metal ions. The title compound is shown in Fig. 1 and it is obvious that there is no center of inversion linking the metal ions. We report detailed variable-temperature absorption spectra and outline the theoretical model to analyze the experimental results in the following.

Experimental

$[Fe^{II}Fe^{III}BPMP(OPr)_2](BPh_4)_2$ was prepared according to method A of ref. 7 with the preparation of the ligand HBPMP following the method given in the same reference. The compounds 2,6-bis(chloromethyl)-4-methylphenol and bis(2-pyridylmethyl)amine were prepared by the procedures in refs 29 and 30, respectively. The identity and purity of the products were ascertained at each stage of the synthesis by ^1H NMR spectroscopy.

Absorption spectra were recorded on a Varian Cary 5E spectrometer with a cooled lead sulfide detector for the near-infrared region. The solution spectra were recorded using 1.011 mM acetone and 9.50 mM d_3-acetonitrile solutions. The solid sample was a polycrystalline film deposited on a 1 mm thick optical quality quartz plate by allowing the solvent in successive drops of a saturated acetonitrile solution of the complex to evaporate slowly under an argon atmosphere. The thickness of the film was estimated as 46 μm from a microscope photograph of ×130 magnification. The quartz plate was mounted on an aluminum mask with a 1 × 3 mm hole. The sample temperature was controlled with a helium gas, continuous-flow cryostat (Oxford Instruments CF1204) with quartz windows.

To determine the intensities of the intervalence band we fitted a Gaussian to the experimental data, using a linear baseline. The integral of the Gaussian was determined numerically by a trapezoidal method. The error margins were determined as described in ref. 31.

Results and discussion

Spectroscopic results

The absorption spectra of the complex in acetone and d_3-acetonitrile solutions are shown in Fig. 2. They clearly show a weak intervalence charge transfer band with a maximum at 7900 cm^{-1} and a molar absorptivity of 120 M^{-1} cm^{-1}. The band position and shape are very similar to those observed in the previously reported spectrum at 22 K in d_3-acetonitrile.[7] The band is at least an order of magnitude weaker than the intervalence band in the Creutz–Taube complex, which has a molar absorptivity of 5000 M^{-1} cm^{-1}.[1]

The absorption spectrum of a solid sample of the complex is presented in Fig. 3. It shows a weak intervalence band with a maximum at 8400 cm^{-1} at 80 K and an estimated molar extinction coefficient of 40 M^{-1} cm^{-1}. While the value of the extinction coefficient is subject to a high error due to uncertainties in the thickness of the polycrystalline layer, it is of the same order of magnitude as in solution. The bandwidths in solution and in the solid are similar, as is the band shape, which is distinctly asymmetric with a steep slope on the high-energy side and a long "tail" on the low-energy side. The intervalence band is very weak in the solid state at 6 K, but becomes stronger with increasing temperature. This suggests a vibronic intensity mechanism. At higher temperatures an additional band starts to appear at about 10 500 cm^{-1}, most likely due to another, higher energy, electronic state. These last two spectroscopic features are not observed in the solution or glass[7] spectra, but are recognizable in the detailed variable-temperature spectra of a crystalline sample.

Calculation of the absorption band shape

Theoretical model. We calculate the absorption band shape of the mixed-valence transition of the title compound from a one-dimensional model involving a transition dipole moment that varies along the configurational coordinate. This model has recently been described[28] and therefore we present here only the most important equations and definitions.

The title compound is a class II compound in the Robin–Day classification.[7,13] The title compound has interchange symmetry, leading to a model that consists of two equivalent, but distinct configurations, as illustrated in Fig. 4. One diabatic potential curve represents the title compound with the Fe^{2+}—B—Fe^{3+} charge distribution, where the excess electron is on the left-hand iron ion; the other potential represents the Fe^{3+}—B—Fe^{2+} charge distribution.

We use a single dimensionless configurational coordinate Q to describe the displacement of the potential minima in order to limit the number of parameters in our model, and conse-

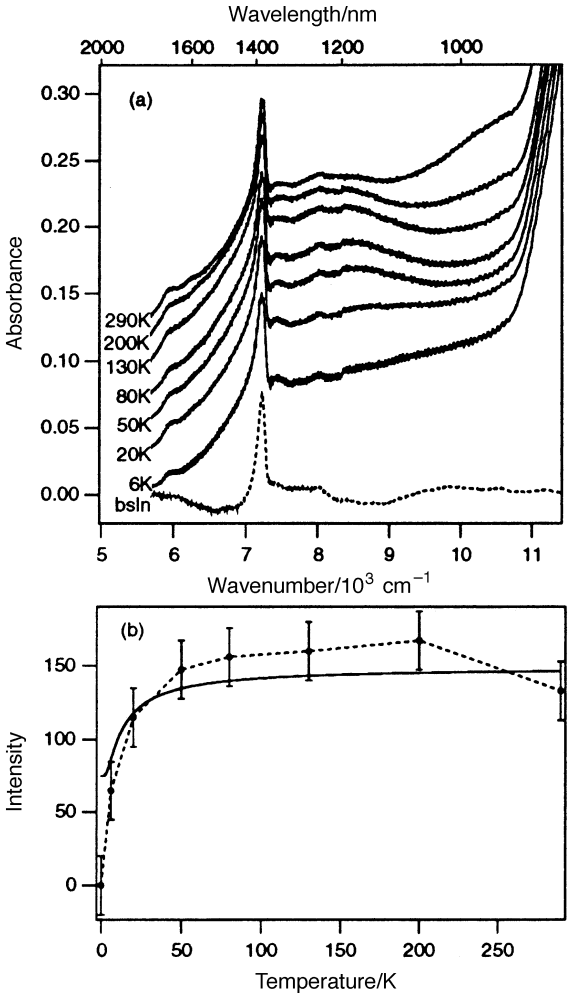

Fig. 3 (*a*) The absorption spectrum of a polycrystalline solid sample of $[Fe^{II}Fe^{III}BPMP(OPr_2)](BPh_4)_2$ in the region of the intervalence band and its variation with temperature. The absorbance scale is for the 6 K spectrum. Spectra are separated by 0.02 absorbance units for clarity. The dotted line shows the absorbance baseline with absorptions due to the cryostat windows. Window absorption causes the sharp peak observed at 7200 cm^{-1}. The modulation observed in the spectra is due to interference from the cryostat windows or quartz plate. (*b*) Integrated intensity of the intervalence band as a function of temperature (dotted line) and the fit to eqn. (10) (solid line).

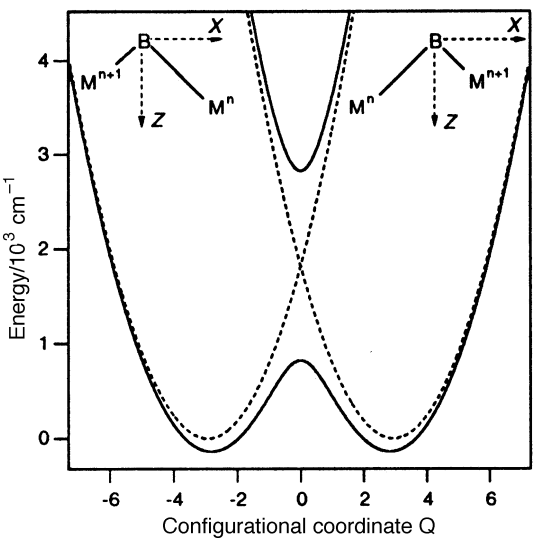

Fig. 4 The diabatic potential surfaces for the time-dependent calculation of the intervalence absorption band of $[Fe^{II}Fe^{III}BPMP(OPr)_2](BPh_4)_2$ (dotted lines). The adiabatic surfaces (solid lines) arise from constant coupling between the diabatic surfaces. The vibrational frequency of both harmonic surfaces is 425 cm^{-1} and their minima are at $\pm$ 2.93 along the dimensionless configurational coordinate Q.

quently the potential energy surfaces and wave functions are one-dimensional. The complex bridging geometry of the title compound (three bridges) is represented by one coordinate, which therefore cannot be attributed to a single vibrational mode. This simplification is often encountered in electron transfer chemistry: an electron transfer reaction is described by a transfer of the system from the initial reactant energy minimum to the final product minimum along the lowest energy path, corresponding to a single reaction coordinate. We use this analogy to reduce the multidimensional problem to a single coordinate and show in the following that the absorption spectrum can be calculated from this simplified model. The nature of our coordinate Q has to be asymmetric in order to link the two configurations corresponding to the potential energy minima, schematically illustrated in Fig. 4. At $Q = 0$ the molecule has a structure with equal M^{n+1}—B—M^n bond lengths and the Z axis bisecting the M^{n+1}—B—M^n angle. It has therefore a mirror plane (through $Q = 0$, containing the Z axis and perpendicular to the X axis). This symmetry aspect distinguishes the title compound from class II molecules with different ligands at the two metal centers and underlines the equivalence of the metal ions in the bent geometry shown schematically in Fig. 4.

We chose harmonic potential curves, but other forms can easily be used with the approach described in the following. The diabatic potential surfaces are given by:

$$V_i(Q) = \tfrac{1}{2}k_i(Q \pm \Delta Q_i)^2 + E_i \qquad (i = 1, 2) \qquad (1)$$

where k_i is the force constant in cm^{-1}, ΔQ_i is the position of the potential minimum along Q in dimensionless units, and E_i is the energy of the potential minimum for the diabatic potential surface, as illustrated in Fig. 4. E_i is chosen to give a lowest-energy eigenvalue of 0 cm^{-1} for the model in Fig. 4. The relation between the force constant $k_{\text{mdyn Å}^{-1}}$ in mdyn $Å^{-1}$ and the force constant k_i in cm^{-1} is: $k_{\text{mdyn Å}^{-1}} = 10^{-1} \cdot k_i^2$.

The method we used to calculate our spectra is based on time-dependent theory. In this approach the absorption spectrum is obtained as the Fourier transform of the autocorrelation $\langle\phi \mid \phi(t)\rangle$. The absorption spectrum is given by:[32,33]

$$I_{\text{abs}}(\omega) = C\omega \int_{-\infty}^{\infty} \exp(i\omega t)\left\{\langle\phi \mid \phi(t)\rangle \times \exp\left(-\Gamma^2 t^2 + \frac{iE_0}{\hbar}t\right)\right\}\mathrm{d}t \qquad (2)$$

$I_{\text{abs}}(\omega)$ is the absorption intensity at frequency ω. Γ is a phenomenological damping factor describing the dephasing of the moving wave packet, most likely due to low-frequency delocalized vibrational modes in a solid. E_0 is the energy of the electronic origin transition. In our model E_o is zero. ϕ is the wave function prepared at $t = 0$ and $\phi(t)$ is the wave function evolving in time as a consequence of the electronic transition. The time-dependent wave function can be visualized as the wave packet propagating on the potential curve of the final state. In our model for intervalence transitions we have to consider two wave packets: one from each potential evolving on the other potential surface. The total autocorrelation $\langle\phi \mid \phi(t)\rangle$ is calculated as:[34]

$$\langle\phi \mid \phi(t)\rangle = \langle\phi_1 \mid \phi_1(t)\rangle + \langle\phi_2 \mid \phi_2(t)\rangle \qquad (3)$$

An important aspect of our model is the definition of the transition dipole moment operator $\hat{\mu}_{i,j}$ for the intervalence transition.[28] The restrictions imposed by symmetry on the restrictions imposed by symmetry on $\hat{\mu}_{i,j}$ are described in ref. 28 and are not identical for class II complexes with "bent" and "linear" structures. In the following, we specifically treat the "bent" structure illustrated in Fig. 4. The wave function ϕ

at time zero is defined as:

$$\phi_i = \phi_i(t = 0) = \hat{\mu}_{i,j}\chi(Q) \quad (i = 1, 2) \tag{4}$$

where $\chi(Q)$ is the eigenfunction of the initial state and $\hat{\mu}_{i,j}$ the transition dipole moment operator. Most literature calculations make the Condon approximation where $\hat{\mu}_{i,j}$ is constant along the configurational coordinate Q, leading to the following operator for $\hat{\mu}_{i,j}$:

$$\hat{\mu}_{i,j} \propto \begin{vmatrix} 0 & 1 \\ 1 & 0 \end{vmatrix} \tag{5}$$

The meaning of this operator is that wave function amplitude is transferred from one diabatic electronic state to the other as a consequence of the interaction with a photon. This operator describes an electric dipole transition that is allowed, resulting in a Z-polarized transition in the coordinate system defined in Fig. 4.[28] X-polarized light induces a transition that is vibronically allowed but strictly forbidden at $Q = 0$.[28] For X-polarized light, $\hat{\mu}_{i,j}$ is not constant along the coordinate Q. The transition dipole moment has to satisfy the following criteria: (1) reflect the interchange symmetry inherent to our model, (2) be zero at $Q = 0$ (electric dipole forbidden) and (3) change sign at the origin, corresponding to an electric dipole forbidden, vibronically allowed transition.[28] Several mathematical forms for $\hat{\mu}_{i,j}$ were suggested.[28,35] We use the form given by Talaga and Zink:[28]

$$\hat{\mu}_{i,j} = \{\exp[\kappa(Q + \Delta Q)^2] - \exp[\kappa(Q - \Delta Q)^2]\} \cdot \begin{vmatrix} 0 & 1 \\ 1 & 0 \end{vmatrix} \tag{6}$$

We use this equation, which constains the adjustable parameter κ, in the following. Fig. 5(*b*) illustrates the shape of this coordinate-dependent transition dipole moment. The transition of Y-polarized light is completely forbidden (vibronically and electronically) at all points along the coordinate Q.[28]

The time-dependent wave function $\phi(t)$ consists, as stated above, of two components arising from each diabatic potential curve. The evolution of this wave packet with time is calculated by solving the time-dependent Schrödinger equation:

$$i\frac{\partial\phi_i}{\partial t} = \begin{pmatrix} H_1 & V_{12} \\ V_{21} & H_2 \end{pmatrix}\begin{pmatrix} \phi_1 \\ \phi_2 \end{pmatrix} \tag{7}$$

In this equation H_i denotes the Hamiltonian for the diabatic basis and V_{ij} is the operator describing the coupling between the two basis states. This matrix is commonly used to represent nonadiabatic intramolecular electron transfer.[36] The delocalization of the electron in our model depends on the coupling between the two diabatic surfaces leading to the adiabatic curves of Fig. 4. Increasing the coupling parameter V_{12} results in a more delocalized situation. We use a coordinate-independent value for $V_{12} = V_{21}$ and the second-order split-operator technique of Feit et al.[37] to solve eqn. (7). This method represents the configurational coordinate Q and the time t by a grid with points separated by ΔQ and Δt, respectively. The time-dependent wave function $\phi(t + \Delta t)$ is obtained from $\phi(t)$ as:

$$\begin{pmatrix} \phi_1(Q, t + \Delta t) \\ \phi_2(Q, t + \Delta t) \end{pmatrix} = \begin{pmatrix} \hat{P}_1 & 0 \\ 0 & \hat{P}_2 \end{pmatrix}\begin{pmatrix} \hat{V}_1 & \hat{V}_{12} \\ \hat{V}_{21} & \hat{V}_2 \end{pmatrix}\begin{pmatrix} \hat{P}_1 & 0 \\ 0 & \hat{P}_2 \end{pmatrix} \times \begin{pmatrix} \phi_1(Q, t) \\ \phi_2(Q, t) \end{pmatrix} + O[(\Delta t)^3] \tag{8}$$

$\hat{P}$ and $\hat{V}$ are the kinetic and potential energy operators, respectively, and are defined in ref. 37. In our diabatic basis, the matrix for the total kinetic energy operator is diagonal and can therefore only propagate a wave function ϕ_i along the diabatic potential energy surface. The matrix for the total potential energy operator is non-diagonal and this operator can transfer wave-packet amplitude between the two diabatic surfaces.

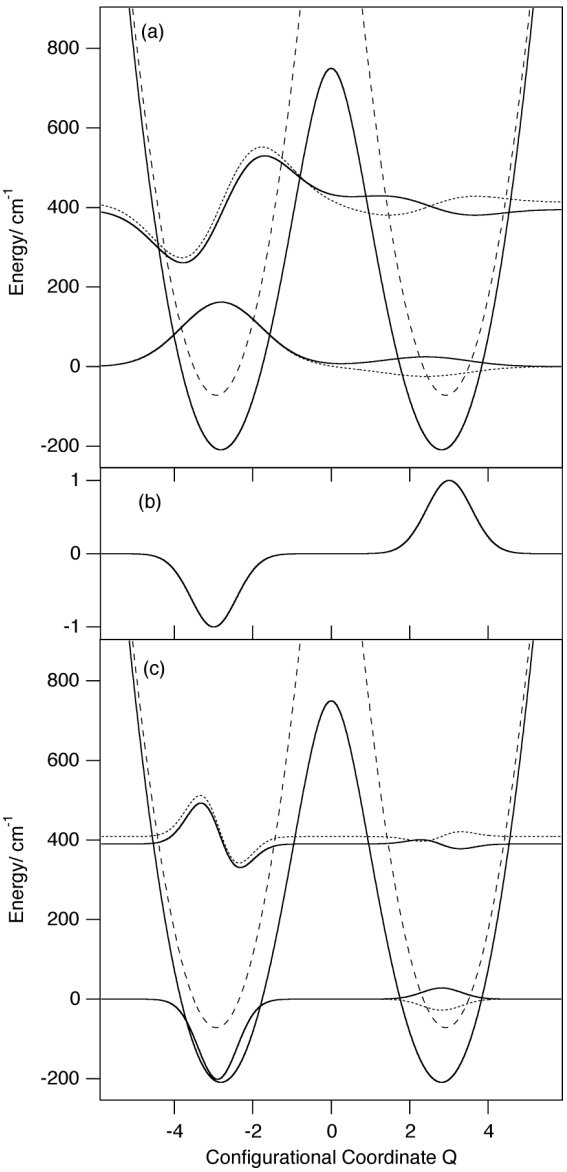

Fig. 5 (*a*) The first four eigenfunctions of the model for the mixed-valence complex are shown as alternating solid and dotted lines. Only the component of each eigenfunction belonging to the potential energy curve on the left is included in the figure. The plots of the eigenfunctions start at the energy of their eigenvalues on the ordinate. (*b*) The coordinate-dependent dipole moment used in our calculations [eqn. (6)]. (*c*) The product of the eigenfunctions (part *a*) and the dipole moment (part *b*). These products are used as the starting wave packets $\phi(t = 0)$ in the time-dependent calculations.

To obtain the eigenfunctions χ_i corresponding to the eigenvalue E_i of the coupled diabatic system, we use:

$$\chi_i(E_i) = \int_0^T \phi(t)w(t)\exp\left(\frac{iE_i}{\hbar}t\right)dt \tag{9}$$

χ_i is again an array with two components corresponding to each diabatic potential energy curve, $\phi(t)$ is the time-dependent propagating wave function and $w(t)$ is a Hanning window function.[37] We calculate the absorption spectrum using a number of eigenfunctions that are propagated on the potential surfaces after multiplication with the transition dipole moment operator described by eqn. (6). We then obtain the absorption spectra at different temperatures as a sum of

individual spectra arising from each level multiplied with the Boltzmann population of the level.

Application to the absorption spectrum of $[Fe^{II}Fe^{III}$-$BPMP(OPr)_2](BPh_4)_2$. The experimental spectrum of the title compound and the vast majority of intervalence spectra reported in the literature consist of a large unresolved absorption band, making it impossible to determine or even estimate from the experimental data the values of all the parameters needed for a complete model. We are forced to use a simplified model for a number of reasons. For instance, there is a large number of vibrational modes that could be relevant in the electron transfer process. We have recently demonstrated the effects of coupling between electronic states represented by multidimensional potential energy surfaces on charge transfer bands.[38] Highly resolved absorption spectra are necessary for such an analysis. Resonance Raman spectroscopy, a technique that could give us information about the individual vibrational modes in the charge transfer process, even if the absorption spectrum is unresolved,[39] is made prohibitively difficult by both the low extinction coefficient of the intervalence band, implying very weak resonance enhancements, and the decomposition of the title compound, even at very low laser powers.[40] The structural changes between the Fe^{2+} and Fe^{3+} sites are large,[7] leading to a large spatial separation of the potential minima in a model. Reliable representations of the surfaces over a large configurational space are therefore needed. Even excited electronic states cannot *a priori* be neglected for the title compound since the onset of an intense visible absorption band is in the same spectral region as the intervalence band, as seen from the spectra in Fig. 2 and 3(*a*).

We calculated the intervalence absorption band using the one-dimensional model described in the preceding section. First, we used the constant transition dipole moment defined by eqn. (5), that is $\hat{\mu}_{i,j}$ for the transition induced by *Z*-polarized light. This choice represents an electric dipole allowed transition. We obtained a good agreement between the maxima of the experimental and the calculated spectrum, but it was not possible simultaneously to match the experimental bandwidth and the whole band shape. The bandwidth of the calculated spectra is always much larger than observed and the onset of the band occurs too low in energy. The intensity of an allowed transition should be temperature independent, which is not the case for the title compound. The intensity increases significantly with increasing temperature, as given in Fig. 3(*b*).

The observed temperature dependence of the intensity shows that the dominant contribution arises from a vibronically allowed transition. We therefore used the coordinate dependent dipole moment[28] in eqn. (6), corresponding to an *X*-polarized vibronic transition, and we obtained a much better agreement between observed and calculated asymmetric band shapes. Absorption spectra polarized along the optical extinction directions are identical to the unpolarized spectra reported in Fig. 3(*a*). This indicates that the molecular axes defined in Fig. 4 do not coincide with the optical crystal axes, preventing us from using polarization to further corroborate our model.

Fig. 6 illustrates the difference between the calculated absorption spectra in the two polarizations. The maximum of the calculated intervalence absorption band is at 7900 and 6500 cm^{-1} for *X* and *Z* polarization, respectively. The band is narrower for the vibronically allowed transition (*X* polarization) than for the fully allowed transition (*Z* polarization). Both calculated spectra show intensity below 1000 cm^{-1}, which is outside our spectroscopic range. These low-frequency transitions are most likely masked by intense vibrational bands.

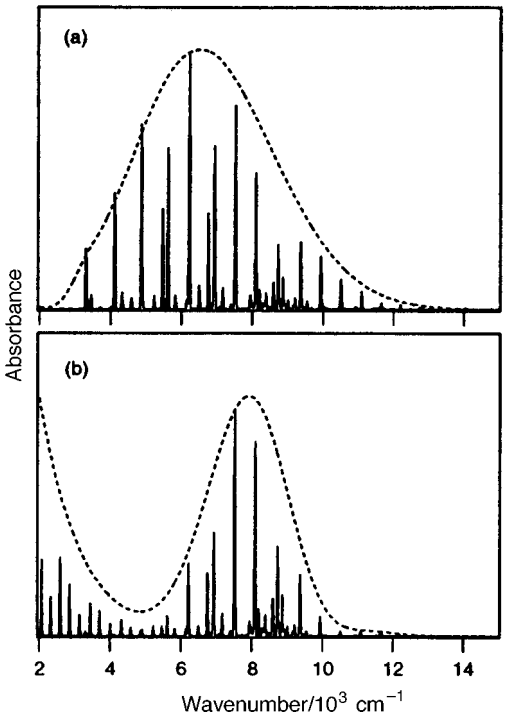

Fig. 6 Calculated absorption spectra based on the potential energy surfaces in Fig. 4 and different transition dipole moments $\hat{\mu}_{i,j}$. Values of 300 cm^{-1} (dotted lines) and 10 cm^{-1} (solid lines) are used for the damping factor Γ. (*a*) *Z*-polarized light: $\hat{\mu}_{i,j}$ is constant. (*b*) *X*-polarized light: $\hat{\mu}_{i,j}$ is the coordinate-dependent function shown in Fig. 5(*b*).

The diabatic and adiabatic potential energy surfaces used for both calculations in Fig. 6 are identical and illustrated in Fig. 4. The diabatic minima are at $\Delta Q = \pm 2.93$. The coupling V_{12} is 1000 cm^{-1} and the vibrational energy for the diabatic potentials is $\nu = 425$ cm^{-1}. A mass of 16 g mol^{-1} (corresponding to the oxygen bridging ligand) in combination with these values leads to a difference of 0.42 Å between the potential minima along the configurational coordinate *Q*. The experimental Fe—ligand bond lengths differ by as much as 0.147 Å, a value on the same order of magnitude as our rough estimate of the difference between the potential minima. Our coupling constant and bandwidth are in the range of the values calculated by Que and coworkers,[7] $V_{12} = 670$ cm^{-1} and $\nu_{1/2} = 4140$ cm^{-1}, using the classical Hush formulas[6] with $\nu_{max} = 7420$ cm^{-1}. The Hush model predicts a bandwidth that is 75% narrower than observed. Using our parameters with the model by Schatz and colleagues,[19,20,41] for compounds with a center of inversion, we obtain a maximum of the intervalence band at 7320 cm^{-1}. This value is close to the observed and our calculated band maxima.

The parameters used to fit the intervalence band for the *X*-polarized transition have rather narrow margins of error. Fig. 7 documents the effect of varying the parameters on the calculated absorption spectra. A decrease of the vibrational frequency ν by only 2% shifts the band maximum to lower energy by 500 cm^{-1}. If the displacement ΔQ is decreased by 5% the maximum shifts to an energy lower by 800 cm^{-1}. Increasing the coupling V_{12} by 10% leads to an intervalence band whose width is much larger than observed in the experiment. A 5% increase of the parameter κ, describing the dipole moment, leads to a shift of 250 cm^{-1} to lower energy.

The most important eigenfunctions χ_i and the products $\chi_i\hat{\mu}_{i,j}$ are shown in Fig. 5. The main effect of the dipole moment $\hat{\mu}_{i,j}$ is to reduce the amplitude near the origin of the coordinate axis. This effect reflects the vibronic transition, which is not allowed at $Q = 0$. Intensity is gained at nonzero values of the enabling mode. In general, we expect the

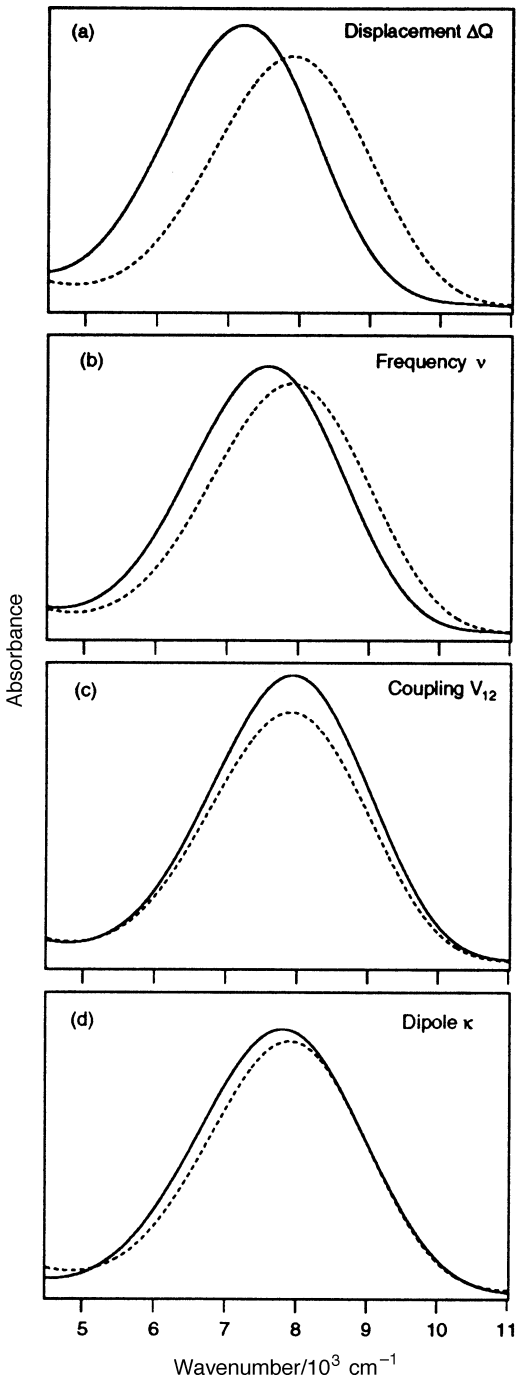

Fig. 7 Calculated absorption spectra using different values for the parameter. (*a*) Coordinate displacement $\Delta Q = 2.93$ (dotted line) and $\Delta Q = 2.78$ (solid line). (*b*) Vibrational frequencies of 425 cm^{-1} (dotted line) and 415 cm^{-1} (solid line) (*c*) Coupling $V_{12} = 1000$ cm^{-1} (dotted line) and $V_{12} = 1100$ cm^{-1} (solid line). (*d*) Width of the coordinate-dependent dipole moment [eqn. (6)] $\kappa = -4.90$ (dotted line) and $\kappa = -5.16$ (solid line).

enabling mode to be different from the coordinate responsible for the band shape, but in our model they are represented by the same coordinate Q. The parameter κ should therefore be considered as a strictly phenomenological quantity. We can estimate the frequency of the most important enabling mode from the temperature dependence of the intervalence band intensities in Fig. 3(*b*). The oscillator strength f of a vibronically allowed electronic transition is given by:[42]

$$f(T) = f^{\circ}\left(1 + \exp\left(-\frac{\nu_{enabl}}{kT}\right)\right) \qquad (10)$$

where f represents the oscillator strength at temperature T, f° is the oscillator strength at $T = 0$ and ν_{enabl} is the frequency of the enabling mode. The fit of f° and ν_{enabl} to the experimental data leads to a value of 7.6 cm^{-1} for the enabling mode. We note that the frequency of the enabling mode is much lower than that of the mode responsible for the main distortion along Q, further underlining that the parameter κ, determining the functional form of the dipole moment, is purely phenomenological. This low-energy enabling vibration is most likely a lattice mode of our crystalline sample. An alternative equation[43] for the temperature dependence of a vibronic band represents the increase as coth ($\nu_{enabl}/2kT$). This equation does not lead to an acceptable fit to the data in Fig. 3(*b*).

Fig. 5(*c*) also shows that the first four eigenvalues are lower in energy than the crossing point of the diabatic surfaces and below the saddle point of the adiabatic surfaces, in accordance with the class II characterization of the title compound.

The first four eigenfunctions are used to calculate the temperature dependence of the absorption band and lead to the result given in Fig. 8. We obtain a good agreement with the observed solid state spectrum of the title compound for temperatures between 80 and 290 K. The absorptions caused by the cryostat windows, shown as the bottom trace in Fig. 3(*a*), have been subtracted from the experimental spectra in Fig. 8 to facilitate the comparison between the observed and calculated spectra. The changes in shape and intensity of the calcu-

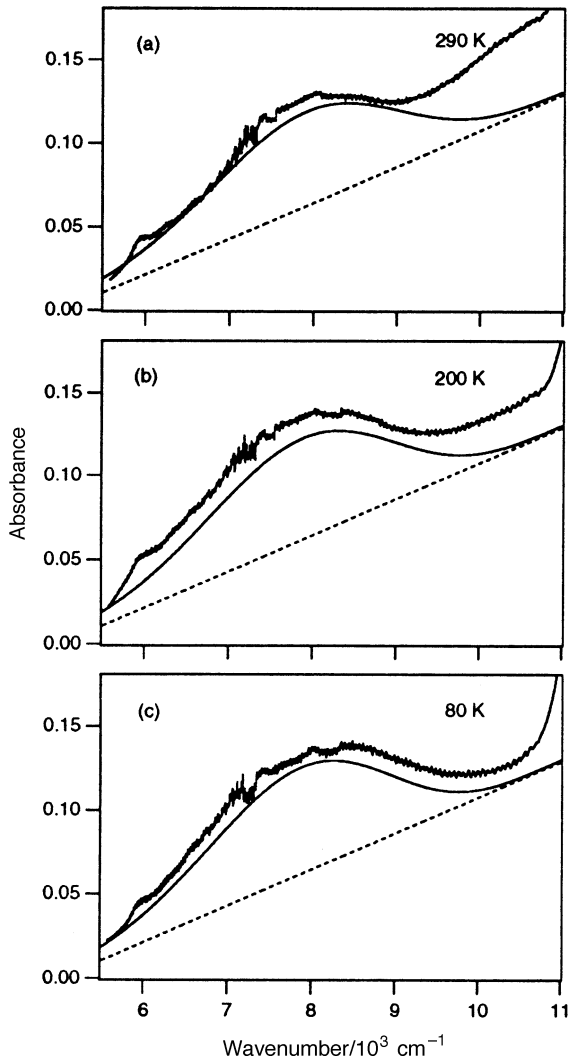

Fig. 8 Comparison of the experimental and calculated intervalence bands. The experimental baseline [dotted trace in Fig. 3(*a*)] is subtracted from the experimental spectrum. The solid line shows the calculated spectrum (offset by 0.01 absorbance units) at 290 K (*a*), 200 K (*b*) and 80 K (*c*). All calculated spectra are obtained with the potential energy surfaces in Fig. 4 and the dipole moment in Fig. 5(*b*). The dotted line shows the baseline used for all calculations.

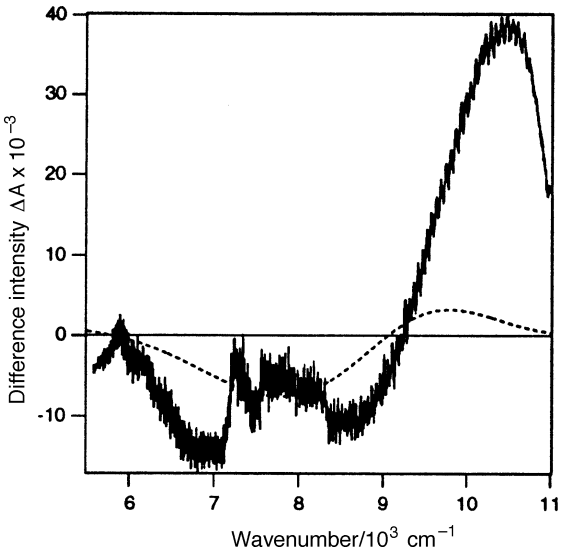

Fig. 9 Difference traces between the spectra at 80 and 290 K in Fig. 8. The solid line denotes the difference between experimental spectra, the dotted line shows the difference between calculated spectra.

lated and experimental spectra in this temperature range show the same tendencies. Fig. 9 compares the difference between experimental spectra at 290 K and 80 K with the difference between the corresponding calculated spectra. Both differences are negative at the low-energy onset of the band, corresponding to an intensity loss at high temperature, and positive at the high-energy end of the intervalence spectrum, corresponding to an intensity gain. The quantitative differences agree well in the low-energy region and are in qualitative correspondence at high energies. Differences traces have been used in the literature to obtain a detailed comparison between experimental and calculated intervalence bands.[44]

Between 6 K and 80 K the spectrum gains considerable intensity, which our model cannot account for, as the Boltzman population of the levels in Fig. 5 does not change significantly between 0 and 80 K. Low-frequency enabling modes would have to be explicitly included in the model to account for this effect.

The analysis of the near-infrared intervalence band of the title compound shows that a one-dimensional model is adequate for the calculation of the band shape. Time-dependent theory provides an approach that allows us explicitly to consider the effects of the transition dipole operator on the calculated spectrum.

Acknowledgements

This work was made possible by grants from the Natural Sciences and Engineering Research Council (Canada).

References

1 C. Creutz and H. Taube, *J. Am. Chem. Soc.*, 1973, **95**, 1086.
2 C. Creutz, *Prog. Inorg. Chem.*, 1983, **30**, 1.
3 N. Sutin, *Prog. Inorg. Chem.*, 1983, **30**, 441.
4 P. Chen and T. J. Meyer, *Chem. Rev.*, 1998, **98**, 1439.
5 R. J. Crutchley, *Adv. Inorg. Chem.*, 1994, **41**, 273.
6 N. S. Hush, *Prog. Inorg. Chem.*, 1967, **8**, 391.
7 A. S. Borovik, V. Papaefthymiou, L. F. Taylor, O. P. Anderson and L. Que, *J. Am. Chem. Soc.*, 1989, **111**, 6183.
8 G. Blondin and J.-J. Girerd, *Chem. Rev.*, 1990, **90**, 1359.
9 D. R. Gamelin, D. W. Randall, M. T. Hay, R. P. Houser, T. C. Mulder, G. W. Canters, S. d. Vries, W. B. T. Y. Lu and E. I. Solomon, *J. Am. Chem. Soc.*, 1998, **120**, 5246.
10 W. M. Laidlaw, R. G. Denning, T. Verbiest, E. Chauchard and A. Persoons, *Nature* (*London*), 1993, **363**, 58.
11 M. D. Ward, *Chem. Soc. Rev.*, 1995, **24**, 121.
12 B. Raveau, C. Michel, M. Hervieu, J. Provost and F. Studer, in *Earlier and Recent Aspects of Superconductivity*, eds. J. G. Bednorz and K. A. Müller, Springer, New York, 1990, p. 66.
13 M. B. Robin and P. Day, *Adv. Inorg. Chem. Radiochem.*, 1967, **10**, 247.
14 C. Creutz, M. D. Newton and N. Sutin, *J. Photochem. Photobiol., A: Chem.*, 1994, **82**, 47.
15 S. F. Nelsen, R. F. Ismagilov and D. R. Powell, *J. Am. Chem. Soc.*, 1998, **120**, 1924.
16 F. W. Vance, R. D. Williams and J. T. Hupp, *Int. Rev. Phys. Chem.*, 1998, **17**, 307.
17 D. H. Oh, M. Sano and S. G. Boxer, *J. Am. Chem. Soc.*, 1991, **113**, 6880.
18 S. F. Nelsen, R. F. Ismagilov and D. A. Trieber, *Science*, 1997, **278**, 846.
19 S. B. Piepho, E. R. Krausz and P. N. Schatz, *J. Am. Chem. Soc.*, 1978, **100**, 2996.
20 K. Y. Wong and P. N. Schatz, *Prog. Inorg. Chem.*, 1981, **28**, 369.
21 A. Ferretti, A. Lami, M. J. Ondrechen and G. Villani, *J. Phys. Chem.*, 1995, **99**, 10484.
22 A. Ferretti, A. Lami and G. Villani, *Inorg. Chem.*, 1998, **37**, 2799.
23 C. J. Calzado, J.-P. Malrieu and J. F. Sanz, *J. Phys. Chem. A.*, 1998, **102**, 3659.
24 J. R. Reimers and N. S. Hush, *Chem, Phys.*, 1995, **197**, 323.
25 Z. Gasyna and P. N. Schatz, *J. Phys. Chem.*, 1996, **100**, 1445.
26 A. R. Rezvani, C. Bensimon, B. Cromp, C. Reber, J. E. Greedan, V. V. Kondratiev and R. J. Crutchley, *Inorg. Chem.*, 1997, **36**, 3322.
27 D. R. Gamelin, E. L. Bominaar, C. Mathonière, M. L. Kirk, K. Wieghardt, J.-J. Girerd and E. I. Solomon, *Inorg. Chem.*, 1996, **35**, 4323.
28 D. S. Talaga and J. I. Zink, *J. Phys. Chem.*, 1996, **100**, 8712.
29 H. P. Berends and D. W. Stephan, *Inorg. Chem.*, 1987, **26**, 749.
30 J. K. Romary, J. D. Barger and J. E. Bunds, *Inorg. Chem.*, 1968, **7**, 1142.
31 W. H. Press, B. P. Flannery, S. A. Teukolsky and W. T. Vetterling, *Numerical Recipes*, Cambridge University Press, Cambridge, 1986, p. 503.
32 E. J. Heller, *Acc. Chem. Res.*, 1981, **14**, 368.
33 J. I. Zink and K.-S. K. Shin, in *Advances in Photochemistry*, eds. D. H. Volman, G. S. Hammond and D. C. Neckers, Wiley, New York, 1991, vol. 16, p. 119.
34 C. Reber and J. I. Zink, *J. Chem. Phys.*, 1992, **96**, 2681.
35 S. Ling, D. G. Imre and E. J. Heller, *J. Phys. Chem.*, 1989, **93**, 7107.
36 G. C. Schatz and M. A. Ratner, *Quantum Mechanics in Chemistry*, Prentice-Hall, Englewoods Cliffs, NJ, 1993, p. 239.
37 M. D. Feit, J. A. Fleck and A. J. Steiger, *J. Comput. Phys.*, 1982, **32**, 3895.
38 B. Cromp, M. Triest, T. Carrington, Jr. and C. Reber, *Spectrochim. Acta A.*, 1999, **55**, 575.
39 J. L. Wootton and J. I. Zink, *J. Phys. Chem.*, 1995, **99**, 7251.
40 J. L. Wootton, private communication.
41 P. N. Schatz and S. B. Piepho, *J. Phys. Chem.*, 1994, **98**, 11226.
42 O. G. Holmes and D. S. McClure, *J. Chem. Phys.*, 1957, **26**, 1686.
43 A. D. Liehr and C. J. Ballhausen, *Phys. Rev.*, 1957, **106**, 1161.
44 L. F. Murga, A. Ferretti, A. Lami, M. J. Ondrechen and G. Villani, *Inorg. Chem. Commun.*, 1998, **1**, 137.

Paper 8/09607D